Quantifying frequency containment reserve using cross-entropy frequency-constrained contingency-state-analysis model

Yuan, Yiping; Liu, Zhou; Chen, Zhe; Hoej Jensen, Kim; Popov, Marjan

DOI
10.1016/j.ijepes.2022.108705

Publication date
2023

Document Version
Final published version

Published in
International Journal of Electrical Power and Energy Systems

Citation (APA)
Yuan, Y., Liu, Z., Chen, Z., Hoej Jensen, K., & Popov, M. (2023). Quantifying frequency containment reserve using cross-entropy frequency-constrained contingency-state-analysis model. *International Journal of Electrical Power and Energy Systems*, *145*, 1-12. Article 108705. https://doi.org/10.1016/j.ijepes.2022.108705

Electrical Power and Energy Systems 145 (2023) 108705

Contents lists available at ScienceDirect

International Journal of Electrical Power and Energy Systems

journal homepage: www.elsevier.com/locate/ijepes

Quantifying frequency containment reserve using cross-entropy frequency-constrained contingency-state-analysis model

Yiping Yuan [a], Zhou Liu [b,*], Zhe Chen [c], Kim Hoej Jensen [b], Marjan Popov [d]

[a] School of Electrical Engineering, Xi'an Jiaotong University, 12480 Shaanxi, Xi'an, China
[b] Department of Grid Compliance, Siemens Gamesa Renewable Energy AS, 2800 Lyngby, Denmark
[c] Department of Energy Technology, Aalborg University, 9200 Aalborg, Denmark
[d] Faculty of EEMCS, Delft University of Technology, 2628 CD Delft, the Netherlands

ARTICLE INFO

Keywords:
Frequency Containment Reserve
Contingency-State-Analysis
Frequency Control
Under-frequency Load Shedding
Cross-Entropy-based Monte Carlo simulation

ABSTRACT

With the increasing penetration of converter-interfaced generators, the frequency containment reserve (FCR) from conventional generators keeps going down, leading to a potential risk of frequency instability under contingencies. Consequently, Converter-interfaced generators are required to provide FCR and participate in the corrective rescheduling. Nevertheless, how to assess the FCR and quantify the adequacy of FCR under contingencies is a big challenge in modern new power system. To address this challenge, a cross-entropy-based frequency-constrained contingency-state-analysis (FC-CSA) model is proposed in this paper. Notably, both frequency control (FC) of units (i.e., conventional synchronous generators and converter-interfaced generators), and under frequency load shedding (UFLS) are incorporated in the primary frequency response. Then a unified system frequency response (SFR) function representing frequency dynamic is derived. This SFR function is extracted and reformulated as a group of mixed-integer linear constraints and participates in the traditional CSA model. Moreover, a set of frequency dynamic indexes, i.e., Expectation of UFLS risk, Expectation of FCR from conventional and converter-interfaced generators, is extended to depict the FCR that the power system requires. These indexes are calculated by the FC-CSA in a cross-entropy-based monte carlo simulation (CE-MCs). Case studies on a modified IEEE 6-bus test system and IEEE 118-bus test system are carried out to demonstrate the effectiveness of the proposed FC-CSA model.

1. Introduction

With the increasing penetration of converter-interfaced generators in power systems, the FCR from conventional generators dominated power systems is declining. As a result, the power system may have inadequate FCR for frequency supporting against potential contingencies. To handle it, Grid-connected converter-interfaced generators are required to maintain a certain number of FCR amount participating in frequency regulation. As for this, it is critical for dispatchers to evaluate the FCR amount produced by different generators under contingencies.

Existing studies on the estimation of FCR are typically focused on the power system operation level. These relevant studies set up a set of frequency constraints and integrate them into existing scheduling problems, e.g., optimal-power-flow (OPF), security-constrained OPF (SC-OPF), transient-constrained OPF (TC-OPF), economic dispatching (ED), unit commitment (UC), etc. [1–4]. Particularly, Ref. [1] proposed a frequency-constrained OPF (FC-OPF) considering the mechanical dynamic of governors. Ref. [2] built up a set of frequency nadir constraints based on the center-of-inertia (COI)-based swing equation [3]. Ref. [4] put forward a TC-OPF model with frequency dynamic and voltage dynamic into consideration. These studies aimed to find an optimal scheduling plan for minimizing the operating cost while keeping conventional units' FCR amount. However, the impact of frequency regulation from converter-interfaced generators is rarely discussed.

Driven by this, some literature discussed the feasibility of frequency regulation produced by converter-interfaced generators during different frequency responses (e.g., inertia response, primary frequency response, secondary frequency response, etc.). Remarkably, the impact of virtual-inertia (VI)-based converter-interfaced generators on UC problems was discussed in [5] and subsequently extended to an enhanced frequency-constrained UC model. The multiple frequency control schemes considering VI control and droop control were investigated in [6] and transferred to a set of convex constraints participating in UC/OPF

* Corresponding author.
E-mail address: zhou.liu@siemensgamesa.com (Z. Liu).

https://doi.org/10.1016/j.ijepes.2022.108705
Received 13 April 2022; Received in revised form 15 July 2022; Accepted 2 October 2022
Available online 20 October 2022

Nomenclature

Indexes and Sets

b	Index of bus
c	Index of converter-interfaced generators
d	Index of load
g	Index of conventional generator
i	Index of UFLS stage
k	Index of linearized hyperplane
s	Index of sampled contingency
$\mathscr{B}$	Index of bus b
$\mathscr{C}$	Set of converter-interfaced generators c
$\mathscr{D}$	Set of system load d
$\mathscr{C}_b$	Subset of converter-interfaced generator located at bus b
$\mathscr{D}_b$	Subset of conventional generators located at bus b
$\mathscr{G}$	Set of conventional generators g
$\mathscr{G}_b$	Subset of conventional generators located at bus b
$\mathscr{K}$	Set of UFLS stages
$\mathscr{S}$	Set of sampled contingency state s

Parameters

H_G	Aggregated inertia of all conventional generators
D_G	Aggregated damping of all conventional generators
R_G	Aggregated droop gain of conventional generators
F_G	Aggregated fraction of turbine output determined by all conventional generators
T_G	Average time constant of all conventional generators
R_C	Aggregated droop gain of droop-controlled converter-interfaced generators
T_C	Time constant of all converter-interfaced generators
H_g	Inertia constant of conventional generator g
D_g	Damping of conventional generator g
R_g	Droop gain of conventional generator g
F_g	Fraction of turbine output determined by conventional generator g
T_g	Time constant of conventional generator g
R_c	Droop gain generated by droop-controlled converter-interfaced generator c
K_g	Mechanical power gain of conventional generator g
K_c	Mechanical power gain of converter-interfaced generator c
T_c	Time constant of converter-interfaced generator c
Δf	Deviation of system frequency
ω_i	Indicator of each UFLS stage, if i th stage UFLS process is activated, $\omega_i = 1$; otherwise, $\omega_i = 0$.
NK	Number of linearized hyperplanes
$\sigma^s_{l,b}$	Generation Shift Distribution Factor (GSDF) of line l and injected power located at bus b
$RoCoF_{max}$	Max Rate-of-Change-of-Frequency (RoCoF)
p_g^{max}	Maximum power of conventional generator g
p_c^{max}	Maximum power of converter-interfaced generator c
Δp_{step}	Mismatch power in frequency deviation case
κ_{voll}	Coefficient of Value-of-Lost-Load (VoLL)
$\tau_{i\in\{g,c,l\}}$	State of equipment $i \in \{g, c, l\}$. If i is online, $\tau_i = 1$, otherwise,$\tau_i = 0$.
$bigM$	Big number for convex relaxation

Variables

Δp_{ufls}	Forced-load-curtailment due to UFLS
Δp^G_{add}	Additional power produced by all conventional generators
Δp^C_{add}	Additional power produced by all converter-interfaced generators
$\Delta p_{ufls,i}$	Forced-load-curtailment at i th UFLS stage
$\Delta p^G_{add,i}$	Additional power produced by all conventional generators at i th UFLS stage
$\Delta p^C_{add,i}$	Additional power produced by all converter-interfaced generators at i th UFLS stage
r^G_{add}	Frequency reserve that all conventional generators can provide
r^C_{add}	Frequency reserve that all converter-interfaced generators can provide
$\Delta p^G_{add,i,g}$	Additional power produced by conventional generator g at the i th UFLS stage
$\Delta p^C_{add,i,c}$	Additional power produced by converter-interfaced generator c at the i th UFLS stage
$p_{g,s}$	Rescheduled power produced by conventional generator g at contingency s
$p_{c,s}$	Rescheduled power produced by converter-interfaced generators c at contingency s
$\Delta p_{d,s}$	Rescheduled power of load s, due to UFLS, at contingency s
$\Delta p_{ufls,i,d,s}$	Forced-load-curtailment of load s, due to the i th UFLS stage, at contingency s

studies. A unified set of frequency dynamic constraints in [7] was applied to UC studies. These constraints consisted of the rate-of-change-of-frequency (RoCoF) restriction, frequency nadir restriction, and FCR restriction. In relevant studies, the calculated corrective results and FCR configurations in [5–7] representing rescheduling processes are generally based on preselected imbalanced power cases, such as a sudden load increase or a failure of the maximum-output-generator. Nevertheless, the availability of the calculated FCR configuration concerning non-preselected power disturbances needs to be further explored. A multi-state model in [8] for assessing the reserve capability of converter-interfaced generators was developed to address it. Moreover, a probabilistic framework for FCR configuration in N-1 security assessment was developed, and a chance-constrained CSA model representing reserve scheduling was put forward [9]. However, the impact of grid-connected converter-interfaced generators using multiple control schemes was rarely discussed. And the applicability of such models in a wide range of potential contingencies might be further quantified.

Motivated by the above challenges, the aim of this paper is to set up a robust method to estimate the adequacy of FCR configurations in a wide range of contingencies in modern new power systems. Some similar works emphasizing Spinning Reserve (SR) assessment are referred to and investigated to achieve this target. Primarily, possible contingencies are generated by the CE-MCs [10] and substituted into the traditional CSA model to estimate the risk of SR configurations. The uncertain output characteristic of converter-interfaced generators was modelled and incorporated into the CSA model, [11]. An accelerated adaptive importance sampling algorithm was used in [12] to sample contingencies against CE-MCs. Then, an improved SR assessment using adaptive importance sampling and the CSA model was carried out. The impact of time-varying contingencies was modelled via sequential CS-MCs, and a refined SR framework considering sequential contingencies was proposed. On this basis, the forecasting error of converter-interfaced generators' output was incorporated into the baseline CSA model [13,14]. Meanwhile, the influence of energy storage system and electric vehicle participating in corrective rescheduling was analyzed [15], and an enhanced CSA model was presented. These studies rarely mention the dynamic frequency requirement of power systems concerning contingencies. To cover that, the frequency control of conventional synchronous generators was introduced into the traditional CSA model [16]. A probabilistic forecasting and decision method in [17] to

assess the FCR allocation of conventional generators was discussed. The proposed CSA models in [10–17] mainly focused on the assessment of SR from a perspective of steady-state active-power balance, where the frequency regulations of different generators, especially for converter-interfaced generators, are rarely investigated.

To comprehensively quantify the FCR adequacy in a wide range of contingencies, a new frequency-constrained CSA (FC-CSA) model is developed in this paper. This model can effectively estimate the expected amount of FCR configuration and potential forced-load-curtailment due to UFLS. It is helpful for dispatchers to build up security FCR management to guarantee frequency dynamic stability under contingencies. Unlike the existing CSA model, two strengthened points in the proposed model are as follows: 1) the frequency control of converter-interfaced generators participating in primary frequency response is considered, and the potential risk of forced-load-curtailment caused by UFLS is incorporated. 2) the influence of the wide-range contingences on the corrective rescheduling considering frequency dynamic is discussed.

To summarize, the main contributions in this paper are listed as follows,

1. An enhanced FC-CSA model is proposed. Both frequency supports provided by conventional and converter-interfaced generators, and UFLS are considered and reformulated as mixed-integer linear constraints, which are further incorporated into the corrective rescheduling under contingencies.
2. To calculate the expectation of FR in a wide range of contingencies, a set of new frequency dynamic indexes, e.g., Expectations of UFLS risk and expectations of FR from different generators, are created. The FC-CSA model within the CE-MCs is applied here to calculate these new frequency indexes.

The rest of the paper is organized as below: Section II analyses the frequency dynamic of SFR; and constructs a group of new frequency dynamic constraints. These reformulated constraints are integrated into the traditional CSA model. Section III creates a new set of frequency indexes and adopts a CE-MCs solution to solve these dynamic indexes. Section VI compares the validity of FC-CSA through case studies, and a conclusion is drawn in Section V.

2. Frequency dynamic under contingencies

2.1. Unified SFR considering UFLS and FC

Considering a step-type mismatch power, denoted by Δp_{step}, due to the outages of several generators under contingencies, the system frequency changes according to the Swing Equation (SE) [6,18–20].

$$2H_G\Delta f^{'}(t)+D_G\Delta f(t)=\Delta p(t) \tag{1}$$

In the corrective rescheduling process, the power regulations from generators and possible forced-load-curtailment, due to UFLS, are rescheduled to migrate the mismatch power. Thus, $\Delta p(t)$ in the right side of (1) can be expressed as,

$$\Delta p(t)=\Delta p_{step}-\underbrace{\left[\Delta p^{G}_{add}(t)+\Delta p^{C}_{add}(t)\right]}_{\text{Part1}}-\underbrace{\Delta p_{ufls}(t)}_{\text{Part2}} \tag{2}$$

In (2), Part 1 represents the frequency regulation provided by conventional generators and converter-interfaced generators; Part 2 represents the UFLS risk if the $\Delta f(t)$ drops to a specific unsafe range. Assuming a droop-controlled FC for these grid-connected generators: $\Delta p^{G}_{add}(t)=L^{-1}[\Phi_G(s)\Delta f(s)\,];\Phi_G(s)=\left(\frac{K_G(1+F_GT_Gs)}{R_G(1+T_Gs)}\right)$ and $\Delta p^{C}_{add}(t)=L^{-1}[\Phi_C(s)\Delta f(s)\,];\Phi_C(s)=\left(\frac{K_C}{R_C(1+T_Cs)}\right)$ [20], then the transfer function of (1) through Laplace transformation can be rewritten as,

$$\begin{cases}(2H_Gs+D_G)\Delta f(s)=\Delta p(s)\\ \Delta p(s)=\dfrac{1}{s}\Delta p_{step}-(\Phi_G(s)+\Phi_C(s)\,)\Delta f(s)-\Delta p_{ufls}(s)\end{cases} \tag{3}$$

where $\Delta f(s),\ \Delta p(s),\ \Delta p_{ufls}(s),\ \Phi_G(s),\ \Phi_C(s)$, respectively, declare the transfer functions of $\Delta f(t),\Delta p(t),\Delta p_{ufls}(t),\Phi_G(t),\ \Phi_C(t)$. Regarding the Part 2 term in (2), $\Delta p_{ufls}(t)$ is a segmented function depending on the system frequency deviation [21–23], $\Delta p_{ufls}(t)=\Delta p_{ufls,i}$; if $\Delta f(t)\in(\Delta f_{ufls,i},\ \Delta f_{ufls,i+1}]$ where i represents the i th UFLS region. Particularly, to reflect the impact of UFLS on the SFR process, (3) can be divided into several stages with each stage representing the diverse frequency dynamic [21–25]. Fig. 1(a) - (b) describe the change of $\Delta f(t),\Delta p(t)$ considering UFLS and FC. Specifically, taking the 2nd SFR region as an example, $\Delta f(t)\in(0.01,0.015]$, then $\Delta p_{ufls,1}$ (Part 2) is tripped, and a specific value of $\Delta p_{add,1}$ (Part 1) has been rescheduled to migrate the remaining mismatch power. Accordingly, the $\Delta f_i(t)$ representing the SFR in the ith region $(\Delta f_{ufls,i},\Delta f_{ufls,i+1}]$ can be derived as below,

$$\begin{cases}(2H_Gs+D_G)\Delta f_i(s)=\Delta p_i(s)\\ \Delta p_i(s)=\dfrac{1}{s}\Delta p_{step,i}-(\Phi_G(s)+\Phi_C(s)\,)\Delta f_i(s)\end{cases} \tag{4}$$

where $\Delta p_{step,i}$ represents evolved mismatch power linked with the ith region. $\Delta p_{step,i}\ =\Delta p_{step}-\Delta p_{add,i}-\Delta p_{ufls,i};\Delta p_{add,i}=$. $\Delta p^{G}_{add,i}+\ \Delta p^{C}_{add,i}$, where $\Delta p^{G}_{add,i}=\frac{K_G}{R_G}(\Delta f_{ufls,i}-\Delta f_{ufls,i+1})$; $\Delta p^{C}_{add,i}=\frac{K_C}{R_C}(\Delta f_{ufls,i}-\Delta f_{ufls,i+1})$. On this basis, the analytical function of $\Delta f_i(t)$ can be calculated through the inverse Laplace transform,

$$\begin{cases}\Delta f_i(t)=\Delta p_{step,i}\curlywedge_{SFR}(t)\\ \curlywedge_{SFR}(t)=\left[\left(\dfrac{R_G}{R_GD_{equ}+1}\right)(1+\alpha e^{-\zeta w_nt}sin(w_rt+\vartheta)\,)\right]\\ \alpha=\sqrt{\dfrac{1-2\zeta w_nT_G+(T_Gw_r)^2}{1-\zeta^2}}\\ w_n=\sqrt{\dfrac{D_GR_G+1}{2H_GR_GT_G}}\\ D_{equ}=D_G+\dfrac{1}{R_C}\\ w_r=w_n\sqrt{1-\zeta^2}\\ \zeta=w_n\left(\dfrac{D_{equ}R_GT_G+2H_GR_G+F_GT_G}{2(D_{equ}R_G+1)}\right)\\ \vartheta=\arctan\left(\dfrac{w_rT_G}{1-\zeta w_nT_G}\right)-\arctan\left(\dfrac{w_r}{-\zeta w_n}\right)\end{cases}\quad\# \tag{5}$$

In (5), the impact of frequency regulation from converter-interfaced generators can be reflected by the change of D_{equ} [6]. Assuming the same time constant T_G for all conventional generators, usually-two orders of magnitude longer than that of converter-interfaced generators: $T_G\gg T_C\approx 0$, [20], and then the expressions of $\{H_G,D_G,\ R_G,F_G,R_C\}$ can be calculated by utilizing (6) as below,

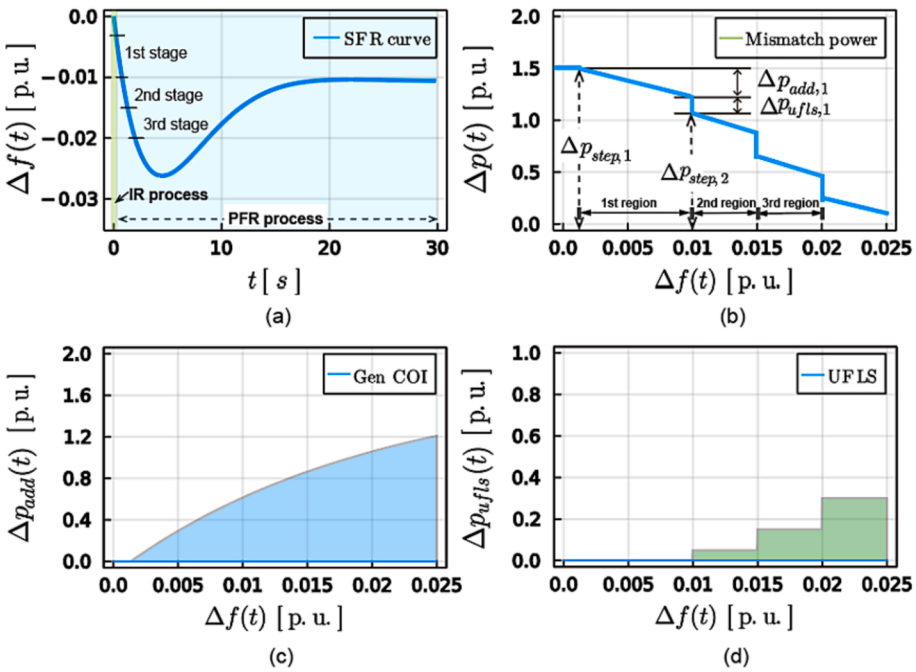

Fig. 1. The dynamic process of SFR in (a); the evolved mismatch power along with the frequency deviation in (b); the change of additional output produced by generators in (c); the forced-load-curtailment, due to UFLS, in (d).

$$\begin{cases} H_G = \sum_{g\in\mathscr{G}} \lambda_g H_g; \\ D_G = \sum_{g\in\mathscr{G}} \lambda_g D_g; \\ \frac{1}{R_G} = \sum_{g\in\mathscr{G}} \lambda_g \frac{K_g}{R_g}; \\ F_G = \sum_{c\in\mathscr{C}} \lambda_c \frac{K_c F_c}{R_c} \\ \frac{1}{R_C} = \sum_{c\in\mathscr{C}} \lambda_c \frac{K_c}{R_c}; \\ \lambda_{i\in\{g,c\}} = \frac{p_i^{max}}{p_{sys}};\ p_{sys} = \sum_{g\in\mathscr{G}} p_g^{max} + \sum_{c\in\mathscr{C}} p_c^{max} \end{cases} \quad \# \tag{6}$$

It is important to note that both additional outputs from grid-connected generators keep zeros (at IR process) until $\Delta f(t)$ is higher than the dead band (e.g., 0.05 Hz). Subsequently, these generators and possible UFLS are successively activated for reducing mismatch power. Fig. 1(c) - (d) illustrate additional outputs of generators and forced-load-curtailment, due to UFLS, along with $\Delta f(t)$. It is clear to find that, due to the segmented feature of UFLS (Fig. 1(d)), $\Delta f(t)$ is divided into several stages in Fig. 1(a). In the 1st stage, only conventional generators and converter-interfaced generators participate in frequency regulation. If $\Delta f(t) \geq 0.01$ p.u., the 2nd stage is activated, and a specific amount of forced-load-curtailment is tripped. Likewise, if $\Delta f(t)$ dips and is lower than 0.015 p.u., the 3rd stage is activated, and another certain amount of forced-load-curtailment is tripped. According to the above discussion, a unified SFR including UFLS and FC from converter-based generators is modelled in (7).

$$\Delta f_i(t) = \begin{cases} \Delta p_{step,1} \swarrow_{SFR}(t), \Delta p_{step,1} = \Delta p_{step}, & \text{if}\, \Delta f_1(t) \in \left(\Delta f_{db}, \Delta f_{ufls,1}\right] \\ \Delta p_{step,2} \swarrow_{SFR}(t), \Delta p_{step,2} = \Delta p_{step,1} - \Delta p_{add,1} - \Delta p_{ufls,1}, & \text{if}\, \Delta f_2(t) \in \left(\Delta f_{ufls,1}, \Delta f_{ufls,2}\right] \\ \Delta p_{step,3} \swarrow_{SFR}(t), \Delta p_{step,3} = \Delta p_{step,2} - \Delta p_{add,2} - \Delta p_{ufls,2}, & \text{if}\, \Delta f_3(t) \in \left(\Delta f_{ufls,2}, \Delta f_{ufls,3}\right] \\ \ldots & \ldots \\ \Delta p_{step,i+1} \swarrow_{SFR}(t) : \Delta p_{step,i+1} = \Delta p_{step,i} - \Delta p_{add,i} - \Delta p_{ufls,i}, & \text{if}\, \Delta f_i(t) \in \left(\Delta f_{ufls,i}, \Delta f_{ufls,i+1}\right] \end{cases} \tag{7}$$

In (7), both grid-connected generators, including conventional and converter-interfaced generators, reduce mismatch power through corrective rescheduling against contingencies. UFLS reduces this deficit via a discretized step forced-load-curtailment. As such, the corrective scheduling of UFLS means that the reduced combination of other frequency supporting cannot keep the system frequency from dropping above the preselected frequency threshold. From this point, the magnitude of forced-load-curtailment, due to UFLS, equals the sum of the system load through the relays chosen to disconnect upon trigger level branch. The solution for choosing suitable disconnected forced-load-curtailment will be further discussed in subsection II. b.

Regarding the time delay of UFLS on the SFR calculating, Ref. [25] compared the impact of the time delay on the control effect of UFLS under different contingencies and found that the time-delay setting might not influence the control effect of UFLS and frequency dynamics if the time-relay is not close to the critical action state of forced-load-curtailment. In other words, if the time delay does not change the total amount of forced-load-curtailment, the time-delay effect is reflected in the delayed action time of forced-load-curtailment, which does not have a significant impact on the residual frequency curves. Similar discussion on the impact of time delay in the UFLS setting can be found in [25,26]. In combination with the above discussion, it is reasonable to believe that the SFR of power system considering UFLS is almost unbiased if the time delay is short enough(usually less than 0.2 s). A more similar discussion on time-delay factors on the SFR modeling is included in the references [24,27].

2.2. Frequency nadir constraint reformulation

To guarantee $\Delta f_i(t)$ within its safe region, the frequency constraint (8) should be held,

$$\Delta f_i(t) \le \Delta f_{ufls,i} \Leftrightarrow \Delta p_{step,i} \le \mathscr{C}_{SFR}^{-1}(t)\Delta f_{ufls,i}, \forall i \tag{8}$$

where (8) denotes the maximum mismatch power in each stage. Especially, if $i = 1$, constraint (8) can be converted as $\Delta p_{step,1} \le \Delta f_{ufls,1}\mathscr{C}_{SFR}^{-1}(t)$. It is an equivalent form of "so-called" frequency safety margin (FSM) [5]. Let $\phi_{SFR} = \max\{\mathscr{C}_{SFR}^{-1}(t)\}$, (8) can be reformulated as,

$$\begin{aligned} &\Delta p_{step,i} \le \phi_{SFR}\Delta f_{ufls,i}, \forall i, \\ &\phi_{SFR} = \mathscr{C}_{SFR}^{-1}(t) : t = \frac{1}{w_r}\tan^{-1}\left(\frac{w_r T_G}{1-\zeta w_n T_G}\right) \end{aligned} \tag{9}$$

It's worth noting that the UFLS is sequentially activated [23]. Hence, to reflect the sequential activated logics of UFLS, a set of binary variables $\mu_i : i \in \{1,2,3\}$ are used to describe the associated power regulations,

$$\Delta p_{step,i} \le \rho_i \phi_{SFR}\Delta f_{ufls,i} + (1-\rho_i)big_M, \forall i \tag{10}$$

$$\rho_i = \mu_i - \mu_{i+1}, \sum_{i\in\mathscr{K}}\rho_i = 1, \mu_i \ge \mu_{i+1}, \forall i \tag{11}$$

where constraint (10) specifies generators' power regulations in each stage. Constraint (11) defines the sequential activated state for each UFLS region. Since the constraint (10) is nonlinear because ϕ_{SFR} in (10) is nonlinear, therefore a group of linear hyperplanes $\mathscr{H}_k\left(H_G^k, \frac{1}{R_G^k}, D_{equ}^k, F_G^k\right) = \alpha_1^k H_G^k + \alpha_2^k(\frac{1}{R_G^k}) + \alpha_3^k D_{equ}^k + \alpha_4^k F_G^k + \alpha_5^k$ is adopted to fit $\phi_{SFR}(H_G, \frac{1}{R_G^k}, D_{equ}, T_G^k)$. Here, $\{H_G^k, \frac{1}{R_G^k}, D_{equ}^k, F_G^k\}$ is a group of sampled evaluation points derived from (6); $\{\alpha_1^k, \alpha_2^k, \alpha_3^k, \alpha_4^k, \alpha_5^k\}$ are the coefficients determined by each hyperplane $\mathscr{H}_k$. The value of coefficients can be estimated by minimizing the loss function: $.Q_{loss}(\alpha_1^k, \alpha_2^k, \alpha_3^k, \alpha_4^k, \alpha_5^k) = \sum_{k=1}^{NK}(\phi_{SFR}(H_G^k, \frac{1}{R_G^k}, D_{equ}^k, F_G^k) - \mathscr{H}_k\left(H_G^k, \frac{1}{R_G^k}, D_{equ}^k, F_G^k\right)^2$, [6]. That is,

$$min : Q_{loss}\left(\alpha_1^k, \alpha_2^k, \alpha_3^k, \alpha_4^k, \alpha_5^k\right) \tag{12}$$

$$s.t., \phi_{SFR}\left(H_G^k, \frac{1}{R_G^k}, D_{equ}^k, F_G^k\right) - \mathscr{H}_k\left(H_G^k, \frac{1}{R_G^k}, D_{equ}^k, F_G^k\right) \ge 0, \ \forall k \tag{13}$$

This is a kind of quadratic programming problem, which can be solved by open-source solver, e.g., Interior-Point-OPTimizer (IPOPT), or commercial solvers, e.g., CPLEX and Gurobi. More details about the convex properties and solution method of ϕ_{SFR} can be referred to [2,6,20]. By substituting $\mathscr{H}_k$ into (10), a set of bilinear constraints can be derived as follows,

$$\Delta p_{step,i} \le \rho_i \mathscr{H}_{k,i}\left(H_G^k, \frac{1}{R_G^k}, D_{equ}^k, F_G^k\right)\Delta f_{ufls,i} + (1-\rho_i)big_M, \ \forall i, \forall k \tag{14}$$

By introducing a slacked variable $z_{k,i}$ representing the product of $\rho_i \mathscr{H}_{k,i}\left(H_G^k, \frac{1}{R_G^k}, D_{equ}^k, F_G^k\right)$, (14) can be converted into a set of desired linear constraints,

$$\Delta p_{step,i} \le z_{k,i}\Delta f_{ufls,i} + (1-\rho_i)big_M, i \in \{1,2,3\}, \ \forall k \tag{15}$$

$$\begin{aligned} &\mathscr{H}_{k,i}\left(H_G^k, \frac{1}{R_G^k}, D_{equ}^k, F_G^k\right) - big_M(1-\rho_i) \le z_{k,i} \\ &\le \mathscr{H}_{k,i}\left(H_G^k, \frac{1}{R_G^k}, D_{equ}^k, F_G^k\right), \ z_{k,i} \in \mathbb{R}^+, \ \forall i, \ \forall k \end{aligned} \tag{16}$$

Accordingly, the complete form of frequency dynamic constraints can be obtained,

$$\Delta p_{step,i} \le z_{k,i}\Delta f_{ufls,i} + (1-\rho_i)big_M, \forall i, \forall k \tag{17}$$

$$\mathscr{H}_{k,i}\left(H_G^k, \frac{1}{R_G^k}, D_{equ}^k, F_G^k\right) - bigM(1-\rho_i) \le z_{k,i} \le \mathscr{H}_{k,i}\left(H_G^k, \frac{1}{R_G^k}, D_{equ}^k, F_G^k\right), \forall i, \forall k \tag{18}$$

$$\rho_i = \mu_i - \mu_{i+1}, \sum_{i\in\mathscr{K}}\rho_i = 1, \mu_i \ge \mu_{i+1}, \forall i, \forall k \tag{19}$$

$$\Delta p_{step,i+1} = \Delta p_{step,i} - \Delta p_{add,i} - \Delta p_{ufls,i}, \forall i \tag{20}$$

$$\Delta p_{add,i} = \Delta p_{add,i}^G + \Delta p_{add,i}^C, \forall i \tag{21}$$

$$\Delta p_{add,i}^G \ge \rho_i \sum_{g\in\mathscr{G}}\Delta p_{add,i,g}^G; \Delta p_{add,i,g}^G \ge \varpi_g \frac{1}{R_g}\Delta f_{ufls,i}, \forall i \tag{22}$$

$$\Delta p_{add,i}^C \ge \rho_i \sum_{c\in\mathscr{C}}\Delta p_{add,i,g}^C; \Delta p_{add,i,g}^C \ge \varpi_c \frac{1}{R_c}\Delta f_{ufls,i}, \forall i \tag{23}$$

$$\sum_{i\in\mathscr{K}}\Delta p_{add,i}^G \le r_{add}^G; \sum_{i\in\mathscr{K}}\Delta p_{add,i}^C \le r_{add}^C, \forall i \tag{24}$$

$$\sum_{i\in\mathscr{K}}\Delta p_{add,i,g}^G \le p_g^{max} - p_g, \forall g \tag{25}$$

$$\sum_{i\in\mathscr{K}}\Delta p_{add,i,c}^C \le p_c^{max} - p_c, \forall c \tag{26}$$

$$\Delta p_{add,i}^G \in \mathbb{R}^+, \Delta p_{add,i}^C \in \mathbb{R}^+, r_{add}^G \in \mathbb{R}^+, r_{add}^C \in \mathbb{R}^+, \tag{27}$$

$$\Delta p_{ufls,i} \in \mathbb{R}^+, r_{add,g} \in \mathbb{R}^+, r_{add,c} \in \mathbb{R}^+, z_{k,i} \in \mathbb{R}^+, \tag{28}$$

$$\rho_i \in \{0,1\}, \mu_i \in \{0,1\} \tag{29}$$

where constraints (17) and (18) define the sufficient limits of the FSM at each UFLS region. Constraint (19) defines the sequentially activated state of UFLS regions. Constraint (20) defines the mismatched power at each UFLS region. Constraint (21) declares the sum of additional outputs from grid-connected generators. Constraint (22) defines

the sum of additional outputs from conventional generators participating in primary frequency response. Likewise, constraint (23) defines the sum of additional outputs from converter-based generators. Constraint (24) enforces the bindings of the additional output from different generators. The bindings define the least amount of the frequency containment reserve for guaranteeing system frequency security against contingencies. Constraints (25) and (26) declare the limits of additional adjustable output for each conventional and converter-based generator. Constraints (27) and (28) define the variable types and feasible space of decision variables. The proposed CSA model considering frequency dynamics can solve both rescheduled outputs from conventional and converter-based generators and discretized forced-load-curtailment due to UFLS. On this basis, by statistically analyzing additional outputs from different types of generators, the binding of FCR configuration for power systems can be smoothly estimated.

To prevent $\Delta f(t)$ from very fast change during the IR process, the RoCoF limit, denoted by $\Delta f^{'}(t); \Delta f^{'}(t) \le RoCoF_{max}$ should be considered. Since the maximum of $\Delta f^{'}(t)$ can be estimated as:$\max\{\frac{1}{2H} \times (\Delta p(t) - D\Delta f(t)\} \le \max\left(\frac{1}{2H}\Delta p(t)\right) \le \frac{1}{2H}\Delta p_{step,1}$. Then, the following constraint can be held, [6].

$$max\{\Delta f^{'}(t)\} \le RoCoF_{max} \Leftrightarrow H_G \le \frac{\Delta p_{step,1}}{2RoCoF_{max}} \tag{31}$$

3. Frequency-Constrained CSA (FC-CSA) model

To guarantee the stability of frequency dynamic under contingency s, the frequency constraints, e.g., (17)-(30), are incorporated in the baseline CSA model. Therefore, an enhanced FC-CSA model can be developed as follows,

$$Q: \min \kappa_{voll} \sum_{d\in\mathscr{D}} \Delta p_{d,s} \tag{31}$$

$$s.t., \sum_{g\in\mathscr{G}} p_{g,s} + \sum_{c\in\mathscr{C}} p_{c,s} + \sum_{d\in\mathscr{D}} \Delta p_{d,s} = \sum_{d\in\mathscr{D}} p_d, \forall g, \forall c, \forall d, \forall s \tag{32}$$

$$-p_l^{max} \le \sum_{b\in\mathscr{B}} \sigma_{l,b}^{s} \left(\sum_{g\in\mathscr{G}(b)} p_{g,s} + \sum_{c\in\mathscr{C}(b)} p_{c,s} + \sum_{d\in\mathscr{D}(b)} \Delta p_{d,s} - \sum_{d\in\mathscr{D}(b)} p_d \right) \le p_l^{max}, \forall l, \ \forall s \tag{33}$$

$$p_g^{min} \le p_{g,s} \le \tau_{g,s} p_g^{max}, \forall g, \forall s \tag{34}$$

$$p_g^{min} \le p_{g,s} \le \tau_{g,s}\left(p_{g,0} + r_{add,g,s}\right), \forall g, \ \forall s \tag{35}$$

$$0 \le p_{c,s} \le \tau_{c,s} p_c^{max}, \forall c, \forall s \tag{36}$$

$$0 \le p_{c,s} \le \tau_{c,s}\left(p_{c,0} + r_{add,c,s}\right), \forall c, \forall s \tag{37}$$

$$\Delta p_{d,s} = \sum_{i\in\mathscr{K}} \Delta p_{ufls,i,d,s}, 0 \le \Delta p_{d,s} \le p_d, \ \forall i, \ \forall d, \forall s \tag{38}$$

$$cons.(17) - (29), cons.(30), \forall i, \forall k \tag{39}$$

In the above formulation, the objective function (31) aims to minimize the forced-load-curtailment risk caused by UFLS in the corrective rescheduling. Constraint (32) enforces the online power balance between generators and demands. Constraint (33) restricts that each transmission line operates within its limit. Constraint (34) declares the maximum and minimum limits of rescheduled output produced by conventional generators. Constraint (35) describes the frequency reserve restriction for each generator. Constraint (36) declares the maximum and minimum output of converter-interfaced generators. Likewise, Constraint (37) defines the adequate frequency reserves of converter-interfaced generators. Constraint (38) defines the risk of UFLS. Furthermore, FC from conventional and converter-interfaced generators in (39) are added.

Note that the proposed FC-CSA focuses on the impact of FCR on corrective rescheduling. Therefore, the chronological rescheduled output of generators is almost dependent on the FC schemes and available frequency regulations in the time interval of seconds. As for this, the limits of ramping constraints, described in minutes or hours, are not considered in this work.

Let $\boldsymbol{\tau}_s = \cup\{\tau_{g,s}, \tau_{c,s}, \tau_{l,s}\}$, $\boldsymbol{x}_s = \cup\{p_{g,s}, p_{c,s}, \Delta p_{d,s}, r_{add,g,s}, r_{add,c,s}\}$, the FC-CSA with the object function $Q(\boldsymbol{x}_s; \boldsymbol{\tau}_s)$ in (31) can be simplified as,

$$\min Q(\boldsymbol{x}_s; \boldsymbol{\tau}_s) : s.t., cons.(32) - (39) \tag{40}$$

The proposed FC-CSA model is a Mixed-Integer Linear Programming (MILP) problem, computed by existing commercial solvers. The operation constraints (32)-(39) are built on a linearized power flow equation for simplification. However, this research can also be extended to an AC-based CSA or related scheduling topics, e.g., OPF, UC, ED, etc.

Compared with the baseline CSA model, the proposed FC-CSA model has three prominent characteristics: 1) The forced-load-curtailment caused by UFLS is incorporated for guaranteeing the frequency dynamic security of corrective rescheduling. 2) The frequency regulation of converter-interfaced generators is considered. 3) The frequency dynamic considering UFLS and FC from the converter-interfaced generator is derived and converted into a new group of mixed-integer linear constraints. These derived frequency constraints can be incorporated into the corrective rescheduling.

4. Quantifying frequency reserve via FC-CSA

As discussed before, both UFLS risk and FCR allocation can be accessed through (40) concerning specific contingency state. Furthermore, to explore the expectation of FCR in a wide-range of contingencies, a CE-MCs solution is used to assess FCR allocation that the system may require. Let $\mathbb{E}(\boldsymbol{x}_s)$ denote the expectation of FCR allocation, where $\boldsymbol{x}_s$ is calculated by using (40). $\mathbb{E}(\boldsymbol{x}_s)$ can be evaluated as,

$$E(\boldsymbol{x}_s) = \sum_{s\in\mathscr{S}} P_{sys,s}(\boldsymbol{\tau}_s; \boldsymbol{u}) Q(\boldsymbol{x}_s; \boldsymbol{\tau}_s) \tag{41}$$

In (41), $\boldsymbol{u} := \{u_i; i \in \{\mathscr{G}, \mathscr{C}, \mathscr{L}\}\}$ represents the Force-Outage-Rate (FOR) of generators and transmission lines; $P_{sys,s}(\boldsymbol{\tau}_s; \boldsymbol{u})$ denotes the probability of sampled contingency s, which can be calculated: $P_{sys,s}(\boldsymbol{\tau}_s; \boldsymbol{u}) = \prod_{i\in\{\mathscr{G},\mathscr{C},\mathscr{L}\}} (1-u_i)^{\tau_{i,s}} (u_i)^{1-\tau_{i,s}}$. According to the definition of (41), we define $e_{\text{ufls}}, e_{\text{fr,G}}, e_{\text{fr,C}}, e_{\text{lolp}}$ as the expectation of UFLS risk, FCR of conventional generators, FCR of converter-based generators, and Lost-of-Load-Probability because of UFLS. These indexes can be expressed as,

$$\begin{cases} e_{\text{ufls}} = \sum_{s\in\mathscr{S}} P_{sys,s}(\boldsymbol{\tau}_s; \boldsymbol{u}) Q\left(e_{\text{ufls,s}}; \boldsymbol{\tau}_s\right) \\ e_{\text{fr,G}} = \sum_{s\in\mathscr{S}} P_{sys,s}(\boldsymbol{\tau}_s; \boldsymbol{u}) Q\left(e_{\text{fr,G,s}}; \boldsymbol{\tau}_s\right) \\ e_{\text{fr,C}} = \sum_{s\in\mathscr{S}} P_{sys,s}(\boldsymbol{\tau}_s; \boldsymbol{u}) Q\left(e_{\text{fr,C,s}}; \boldsymbol{\tau}_s\right) \\ e_{\text{lolp}} = \sum_{s\in\mathscr{S}} P_{sys,s}(\boldsymbol{\tau}_s; \boldsymbol{u}) H\left(e_{\text{ufls,s}}; \boldsymbol{\tau}_s\right) \end{cases} \tag{42}$$

In (42), $e_{\text{ufls,s}} = \sum_{d\in\mathscr{D}} \Delta p_{d,s}$; $e_{\text{fr,G,s}} = \sum_{g\in\mathscr{G}} r_{add,g,s}$; $e_{\text{fr,G,s}} = \sum_{c\in\mathscr{C}} r_{add,c,s}$; $H\left(e_{\text{ufls,s}}\right) = 1$, if $e_{\text{ufls,s}} > 0$; otherwise, $e_{\text{ufls,s}} = 0$. The result of $\{\Delta p_{d,s}, r_{add,g,s}, r_{add,c,s}\}$ can be soluted by utilizing (40). Especially, the physical significance of these extended indexes aims to describe the adequacy of corrective rescheduling concerning system frequency securities in a wide range of contingencies. With the help of these calculated indexes, the ability of the operating state to copy with occasional contingencies can be comprehensively quantified. Furthermore, these indexes about FCRs can be taken as a reference for dispatchers to deploy FCR configuration more reasonably. Since these indicators are built on a statistical

Table 1
The calculation process of frequency reserve allocation.

Pseudo Code: the CE-MCs solution for the proposed model
1) Input: the forced-outage-rate (FOR) data of generators and transmission lines. operation data of generators, transmission lines and system load. Smooth coefficient α
Step 1: Pre-sampling process
2) Generating a set of contingencies $\boldsymbol{\tau}_1, \boldsymbol{\tau}_2, \boldsymbol{\tau}_s, \cdots, \boldsymbol{\tau}_N$ from the $P_{sys,s}(\boldsymbol{\tau}_s;\boldsymbol{u})$; counter $k=1$.
3) Calculating $Q(\boldsymbol{x}_s;\boldsymbol{\tau}_s)$ through (40) for each contingency s, and forming a queue $S=\{Q(\boldsymbol{x}_1;\boldsymbol{\tau}_1), Q(\boldsymbol{x}_2;\boldsymbol{\tau}_2), \cdots, Q(\boldsymbol{x}_s;\boldsymbol{\tau}_s), \cdots, Q(\boldsymbol{x}_{N-1};\boldsymbol{\tau}_{N-1}), Q(\boldsymbol{x}_N;\boldsymbol{\tau}_N)\}$.
4) Using the same sample to update the twisted reference parameter $\boldsymbol{v}=\{(v_i)^k; i\in\{\mathscr{G},\mathscr{C},\mathscr{L}\}\}$: $(v_i)^k=(1-\alpha)(v_i)^{k-1}+\alpha\left(1-\frac{\sum_{s\in\mathscr{S}}P_{sys,s}(\boldsymbol{\tau}_s;n,\boldsymbol{u})H(Q(\boldsymbol{x}_s;\boldsymbol{\tau}_s))\tau_{i,s}}{\sum_{s\in\mathscr{S}}P_{sys,s}(\boldsymbol{\tau}_s;n,\boldsymbol{u})H(Q(\boldsymbol{x}_s;\boldsymbol{\tau}_s))}\right): i\in\{\mathscr{G},\mathscr{C},\mathscr{L}\}$where $H(Q(\boldsymbol{x}_s;\boldsymbol{\tau}_s))$ is a feature function: if $Q(\boldsymbol{x}_s;\boldsymbol{\tau}_s)=0$, $H(Q(\boldsymbol{x}_s;\boldsymbol{\tau}_s))=0$; otherwise,$H(Q(\boldsymbol{x}_s;\boldsymbol{\tau}_s))=1$.
5) Sorting S with an increasing order. Let $L_k:=Q_{\lfloor(1-\rho)N\rfloor}$ denotes a ρ-quantile of S. If $L_k\geq 0$, the pre-sampling process is finished, and jump to Step-2. Otherwise, let $k=k+1$, and jump to 2) in Step-1.
Step 2: CE-MCS sampling process
6) Replacing $\boldsymbol{v}$ with $\boldsymbol{u}$, and reset counter $k=1$.
7) Generating the contingency s through $P_{sys,s}(\boldsymbol{\tau}_s;n,\boldsymbol{v})$ with each component's state denoted by $\boldsymbol{\tau}_{i,s}: i\in\{\mathscr{G},\mathscr{C},\mathscr{L}\}$.
8) Evaluating $Q(\boldsymbol{x}_s;\boldsymbol{\tau}_s)$ via (40) and calculating the unbiased value of $\{e_{\text{ufls}}, e_{\text{fpr,G}}, e_{\text{fpr,C}}\}$ according to (42).
9) Checking the variance coefficients of UFLS index, denoted by $\beta_{\text{ufls}}:\beta_{\text{ufls}}=\sigma(e_{\text{ufls}})/\mathbb{E}(e_{\text{ufls}})$. If it is not greater than β_{max}, terminate the CE-MCS process and save the value of $\{e_{\text{ufls}}, e_{pfr.G}, e_{\text{pfr,C}}, e_{\text{lolp}}\}$, otherwise, $k=$ k +1, and then jump to 7).

expectation of corrective rescheduling concerning wide-range contingencies, these indexes overcome the conservatism caused by analyzing the most serious contingences alone to some extent. Meanwhile, it would be more conducive to realize the coordination of operation economy and security, especially for frequency security issues.

Although the system frequency security concerning the most severe contingency may be feasible, nevertheless, it is conservative to emphasize frequency security only against severe contingencies. Notably, the frequency insecurity issues concerning serious contingencies are usually rare. And we still set aside frequency containment reserve (FCR) to cope with these contingencies. Thus, the system will keep a large amount of FCR if the frequency security regarding the most severe contingency is taken as the unique criterion to guarantee the system frequency security. It is not very economical because the system may never operate the most severe contingencies. Notice that the impact of frequency dynamic requirement on the supply–demand balance and scheduling feasibility become more and more difficult with the increase in penetration of uncertain resources. To reflect that, the power system needs to combine each generator's frequency control characteristic and set up a suitable FCR amount under stochastic contingencies. Hence, the expectation of FCR in a wide range of contingencies actually reflects the actual frequency dynamic requirement against contingencies. Accordingly, it is a relatively robust solution to achieve suitable FCR management by quantifying the security risk and probability in a wide range of contingencies.

Since system failure is rare, the calculational process via (42) would be computationally demanding. To accelerate the calculation process, the CE-MCs [24] is implemented. The contingency s is sampled from a designed proposed distribution $P_{sys,s}(\boldsymbol{\tau}_s;\boldsymbol{v})$ instead of $P_{sys,s}(\boldsymbol{\tau}_s;\boldsymbol{u})$, and a related likelihood $w(\boldsymbol{\tau}_s;\boldsymbol{u},\boldsymbol{v})$ is calculated to keep the unbiases of estimator. As for this, e_{ufls} can be rewritten as,

$$e_{\text{ufls}}=\sum_{s\in\mathscr{S}}w(\boldsymbol{\tau}_s;\boldsymbol{u},\boldsymbol{v})\left(P_{sys,s}(\boldsymbol{\tau}_s;\boldsymbol{v})Q\left(e_{\text{ufls,s}};\boldsymbol{\tau}_s\right)\right): w(\boldsymbol{\tau}_s;\boldsymbol{u},\boldsymbol{v})=\frac{P_{sys,s}(\boldsymbol{\tau}_s;\boldsymbol{u})}{P_{sys,s}(\boldsymbol{\tau}_s;\boldsymbol{v})}=\frac{\prod_{i\in\{\mathscr{G},\mathscr{C},\mathscr{L}\}}(1-u_i)^{\tau_{i,s}}(u_i)^{1-\tau_{i,s}}}{\prod_{i\in\{\mathscr{G},\mathscr{C},\mathscr{L}\}}(1-v_i)^{\tau_{i,s}}(v_i)^{1-\tau_{i,s}}} \tag{43}$$

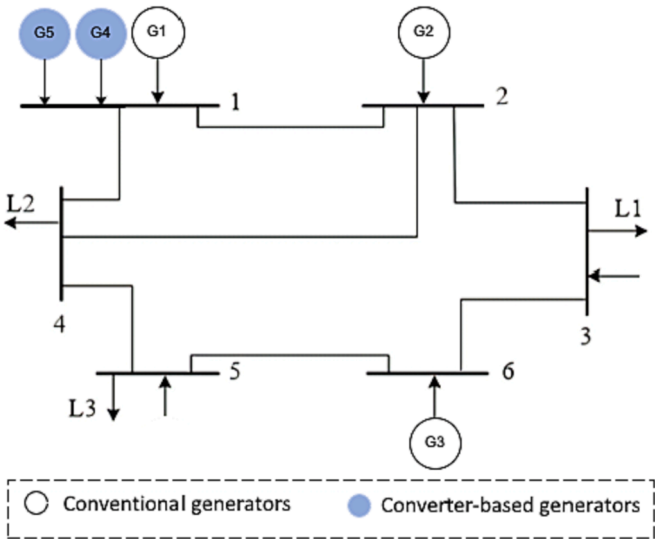

Fig. 2. The single-line diagrams of modified IEEE 6-bus test power system.

Table 2
Both reliability performance parameters of different generators and transmission lines in IEEE 6 bus test system.

Gen.NO.	Type of generators	λ	μ	u
G1	Thermal	2.0	248.0	0.005
G2	Thermal	5.0	195.0	0.025
G3	Thermal	10.0	194.0	0.049
G4	Wind turbine	20.0	120.0	0.143
G5	Wind turbine	20.0	120.0	0.143

Table 3
The frequency parameters of different generators in IEEE 6 bus test system.

Gen.NO.	H	K	F	R	D	T
G1	7	0.90	0.15	0.04	0.06	8.00
G2	5.5	0.95	0.35	0.03	0.1	8.00
G3	3.5	0.98	0.25	0.05	0.18	8.00
G4	—	1.00	—	0.04	—	0.06
G5	—	1.00	—	0.04	—	0.06

The calculation of $e_{\text{fr,G}}, e_{\text{fr,C}}, e_{\text{lolp}}$ is similar as e_{ufls} in (43). Table 1 lists the pseudo code for calculating frequency indexes.

5. Case studies and analysis

This section uses two cases, including a modified version of the IEEE 6-bus system and the IEEE 118-bus system, to check the validity of the proposed FC-CSA. Both cases are coded in Julia 1.6.8/JuMP environment [29] using Gurobi 9.0.3 on a personal Desktop with Intel(R) Core (TM) i7-8700 CPU and RAM 12.0 GB.

1) IEEE 6-bus test system.
2) Boundary data description.

The system comprises 6 buses, 7 lines, and 3 conventional generators

[30]. The total installed capacity of conventional generators is 240MW. The system also contains 2 wind farms located on bus 1, with each farm's capacity set to be 50MW. In such settings, the percent of converter-interfaced generators for all generators' total installed capacity is 29.40%. Besides, the baseline value of the power is 100.00 MW and the baseline value of system frequency is 50.00 Hz. Fig. 2 illustrates the single-line diagram of applied IEEE 6-bus system. Table 2 declares the reliability performance parameters of different generators that consist of FOR λ, repair ratio μ, and unavailability u. Based on this assumption, the unavailability u of each generator can be evaluated as $u = \lambda/(\lambda + \mu)$, as shown in the 3rd column of Table 3.

Regarding FCR generated by different generators, all grid-connected generators are assumed to take droop control. Table 3 lists related parameters of different controllers [2,5,6], The dead-band of controllers is 0.05 Hz (0.001p.u.); the threshold of ROCOF is 5 Hz/s (0.1 p.u.); the maximum frequency deviation without UFLS activities is 0.50 Hz (0.010p.u.) [26]. It also means that if the deviation of system frequency ranges between [0.001 p.u., 0.010 p.u.], only generators are acquired to participate in frequency regulation. Correspondingly, if the frequency deviation surpluses 0.010 p.u., UFLS will be activated to reduce the mismatch power. Participially, if $\Delta f(t)$ changes between [0.010 p.u., 0.015 p.u.], the 1st stage UFLS (0.1 p. u., equals 5.00 % of system demand) is tripped. Likewise, if $\Delta f(t)$ changes between [0.015 p. u., 0.02 p. u.], the 2nd stage is activated, and 10 % of system load is tripped. The activated states of UFLS along with $\Delta f(t)$ can be referred to Fig. 1(d), in section II.A.

In terms of the computational process of the proposed model, the maximum number of iterations is 1e6. The variance coefficient of e_{ufls}, is taken as the reference to determine whether the algorithm is terminated. If $\beta_{\text{ufls}} \leq 5\%$ or the iteration number is greater than 1e5, the solution of CE-MCs will be terminated.

3) Traditional CSA(*T*-CSA) vs FC-CSA.

To compare the performance of T-CSA (benchmark) [28] and FC-CSA (the proposed model), a contingency scenario with a failure of generator is used to check these models. The contingency scenario used by these models is identical, ensuring that both models have the same boundary data. More detailed, a failure of generator numbered G1 is taken as a contingency scenario, and the result of steady-state OPF is taken as boundary data representing all generators' initial output. Accordingly, Table 4 gives the corrective results solved by the T-CSA and the FC-CSA.

Both corrective results soluted by T-CSA and FC-CSA are different, mainly in the rescheduled output of converter-interfaced generators. Besides, a certain amount of load (0.10 p.u.) in FC-CSA is tripped, while *T*-CSA does not. It is because FC-CSA considers the FC of generators, but *T*-CSA does not. The failure of G1 instantaneously results in a mismatch power (1.02 p. u.) and a change in system frequency. As for this, both conventional generators and converter-interfaced generators are rescheduled to adjust their outputs in combination with their FC controllers. In this region, both additional outputs of different generators are, respectively, [0.00, 0.24, 0.20, 0.25, 0.25]. It can be found that the sum of frequency regulations cannot cover the mismatch power, hence, the frequency deviation will increase and the 2nd UFLS will be activated. During this region, a certain amount of forced-load-curtailment (0.10p. u.) is tripped. This rescheduled process is explained in FC-CSA but implicitly ignored in T-CSA. Another difference between T-CSA and FC-CSA lies in the distribution of FCR allocation. Compared with the initial output at the steady-state, the corrective outputs of conventional generators solved by T-CSA decrease, while the ones of converter-interfaced generators increase. It reflects that the mismatch power is mostly taken up by converter-interfaced generators. Nevertheless, in the FC-CSA model, the corrective outputs of all generators rise, which is consistent with their FC logicisms. In other words, all grid-connected generators have consistency in frequency regulations and increase their outputs for migrating the mismatch power. It has been well explained in the FC-CSA, as shown in the sixth column of Table 4.

Table 4
Both Rescheduled outputs and UFLS risk for this contingency state in IEEE 6 bus test system.

Gen.NO.	$p_{i,0}$ [p.u.]	Benchmark		Proposed model	
		$p_{i,s}$ [p.u.]	$p_{i,s} - p_{i,0}$ [p. u.]	$p_{i,s}$ [p.u.]	$p_{i,s} - p_{i,0}$ [p. u.]
G1 (failed)	0	0	0	0	0
G2	0.4981	0.4059	Negative	0.7834	Positive
G3	0.0996	0.0812	Negative	0.2018	Positive
G4	0.2491	1.0000	Positive	0.5189	Positive
G5	0.2491	0.7048	Positive	0.5189	Positive
UFLS	0	0	Zero	0.1000	Positive

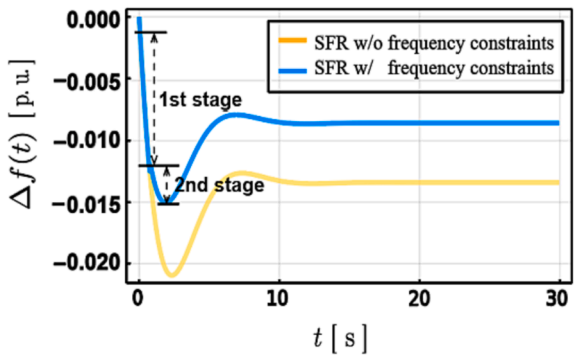

Fig. 3. The SFR curve without ("w/o") frequency constraints in T-CSA and with ("w/") frequency constraints in FC-CSA.

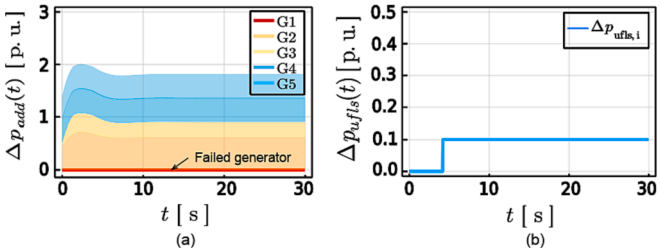

Fig. 4. Both corrected output of generators and forced-load-curtailment due to UFLS under frequency dynamic process.

For analyzing the influence of FCR from converter-interfaced generators and UFLS on frequency dynamics, Fig. 3 simulates the SFR curve with (short as "w/") and without (short as "w/o") considering frequency constraints. The SFR including frequency constraints keeps smaller frequency deviation, resulting in smoother system frequency response. It also justifies the benefit of power regulation from converter-interfaced generators and UFLS. The SFR in the proposed model can be divided into two stages: 1) in the 1st stage, all generators' outputs are rescheduled but no forced-load-curtailment is activated. When the frequency drops to the threshold of 1st UFLS region, the 2nd stage is activated. And a certain number of loads, because of UFLS, is tripped. During this stage, the sum of additional power (0.94p. u.) and forced-load-curtailment (0.10p. u.) is greater than the mismatch power (1.02 p.u.), therefore, the mismatch power is positive, leading to a recovery in system frequency change. Both additional outputs from different generators and UFLS can be found in Fig. 4. According to (42) and Table 6, $e_{\text{ufls,s}} = 0.10\text{p.u.}; e_{\text{fr,G,s}} = 0.34\text{p.u.}; e_{\text{fr,C,s}} = 0.50$ p.u.

In combination with the above discussions, a conclusion can be drawn that the corrective result in T-CSA is conservative because it simply analyzes the rescheduling from a power balance perspective. Conversely, the FC-CSA considers the frequency dynamic and power

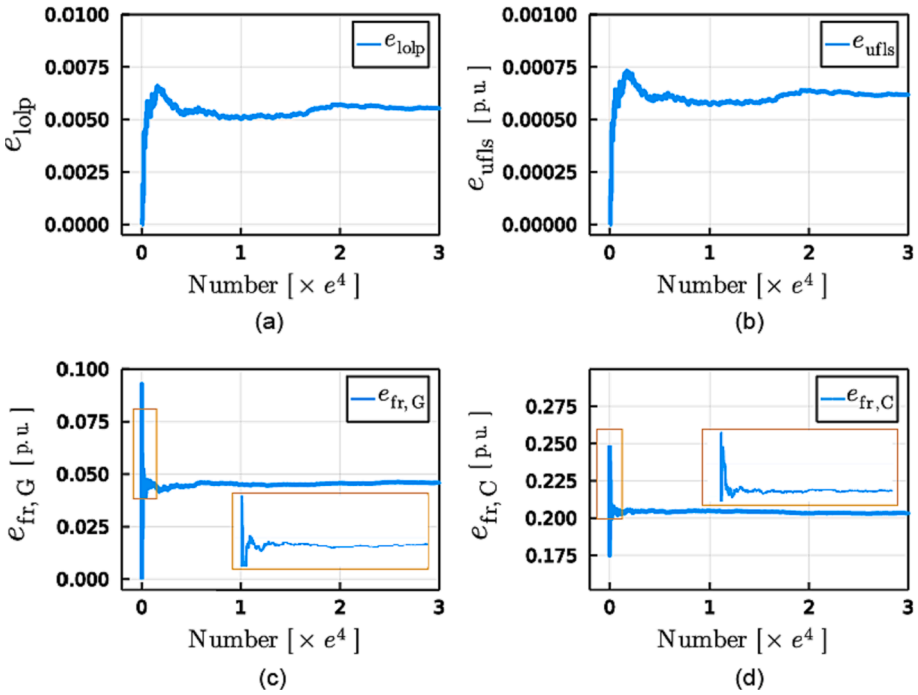

Fig. 5. The calculation process of $e_{\text{lolp}}, e_{\text{ufls}}, e_{\text{fr,G}}, e_{\text{fr,C}}$ produced by FC-CSA in the 6-bus test system.

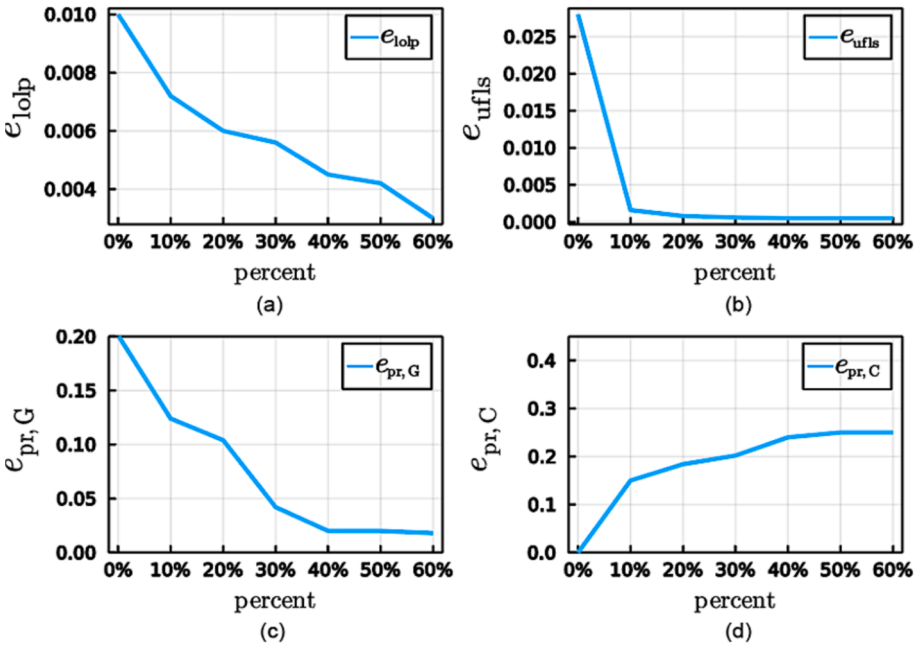

Fig. 6. The change of $e_{\text{lolp}}, e_{\text{ufls}}, e_{\text{fr,G}}, e_{\text{fr,C}}$ along with the increasing percent of converter-interfaced generators.

regulations from all generators. As for this, the proposed FC-CSA is more practical.

4) Quantifying FCR allocation and UFLS.

To provide a comprehensive measure concerning FCR, Fig. 5 illustrates the expectation of UFLS and FCR. the LOLP index and UFLS index are 0.0056 and 0.0006p. u., respectively. The FCR provided by conventional and converter-interfaced generators is 0.042p. u. and 0.202p. u., respectively. This result provides a reference for FCR configuration against frequency deviations.

To investigate the change of FCR at different penetration rates, Fig. 6 statistics the results of $e_{\text{lolp}}, e_{\text{ufls}}, e_{\text{fr,G}}, e_{\text{fr,C}}$ along with the increasing percent of converter-interfaced generators. It is clear to see that both LOLP and forced-load-curtailment, due to UFLS, go down along with an increasing percentage of converter-interfaced generators. Especially, when the associated percentage is zero (0.00 %), e_{lolp}=0.010; e_{ufls}=0.028, which indicates a higher risk of UFLS if relying solely on conventional generators to provide frequency support. when the percentage raises from 0.00 % to 30.00 %,$e_{\text{lolp}} \in [0.005, 0.01]$; $e_{\text{ufls}} \in [0.0006, 0.03]$; $e_{\text{fr,G}} \in .[0.03, 0.20]$; $e_{\text{fr,C}} \in [0.00, 0.25]$. In this situation, the risk of FCR from conventional generators decreases,

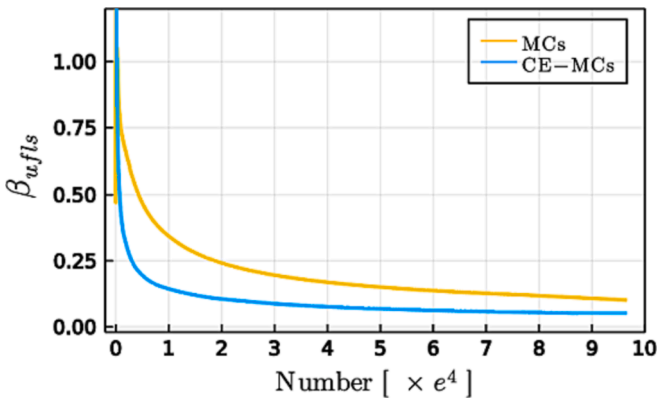

Fig. 7. The calculation process of variance coefficient soluted by conventional MCs and CE-MCs concerning the proposed FC-CSA.

and the reserve from converter-interfaced generators rises. It shows that the system frequency stability can be improved if the FCR from converter-interfaced generators is incorporated. Therefore, the benefit of frequency regulation produced by converter-interfaced generators is verified.

5) Calculational performance analysis.

To check the computational performance of FC-CSA in a CE-MCs framework, a conventional MCs is taken as a baseline to compare with the calculational time of CE-MCs. To ensure the variance coefficient converges to a preselected degree (5 %), 460, 138 iterations (38.24 min of computation time) are required using MCs. Nevertheless, CE-MCs require only 94, 792 iterations (8.87 min). It declares the benefit of CE-MCs in this work. Fig. 7 compares convergence processes of variance coefficients of MCs and CE-MCs. It can be found that CE-MCs has better convergence performance, thus achieving faster computational performance.

6) IEEE 118 bus test system.

A modified IEEE 118 bus system is used to test the scalability of FC-CSA. This system consists of 54 conventional generators, 186 lines, and 91 loads [5,20]. The installed capacity of conventional generators is 7, 220 MW, with a peak-load of 5,516.08MW. Besides, this system consists of three wind farms denoted by G55, G56, and G57. These farms are located at bus {24, 25, 26}, with each capacity assumed to be 500MW. Fig. 8 shows the single-line diagram of modified 118-bus test power system. In such settings, the percent of wind farms for this system's peak-load is 20.79%. Furthermore, the sudden increases of load (approximately 20%) represents the mismatch power under frequency deviation cases. Table 5 gives UFLS risks and rescheduled output of generators. Table 5I describes the number of generators participating in power regulation. Fig. 7 shows UFLS risks and (frequency) reserve allocation of the power system. Fig. 8 shows the iteration process of FC-CSA solved by baseline MCs and CE-MCs, respectively.

It can be found that both sums of generators' additional output by

Table 5
Both rescheduled outputs of generators and UFLS risk under contingency state.

Model	$e_{ufls,s}$ [p. u.]	$e_{fr,G,s}$ [p. u.]	$e_{fr,G,s}$ [p. u.]	$e_{fr,G,s} + e_{fr,G,s}$ [p. u.]
T-CSA	0	8.7902	0	8.7902
FC-CSA	0	6.7763	2.0139	8.7902

Table 6
The number of rescheduled generators participating in corrective rescheduling solved by T-CSA and FC-CSA.

Model	Rescheduled generators
T-CSA	G4, G5, G7, G14-G17, G19-G22, G24-G27, G29, G30, G36, G37, G39, G42-G44, G47, G48, G50-G51
FC-CSA	G1-G54, G55-G57

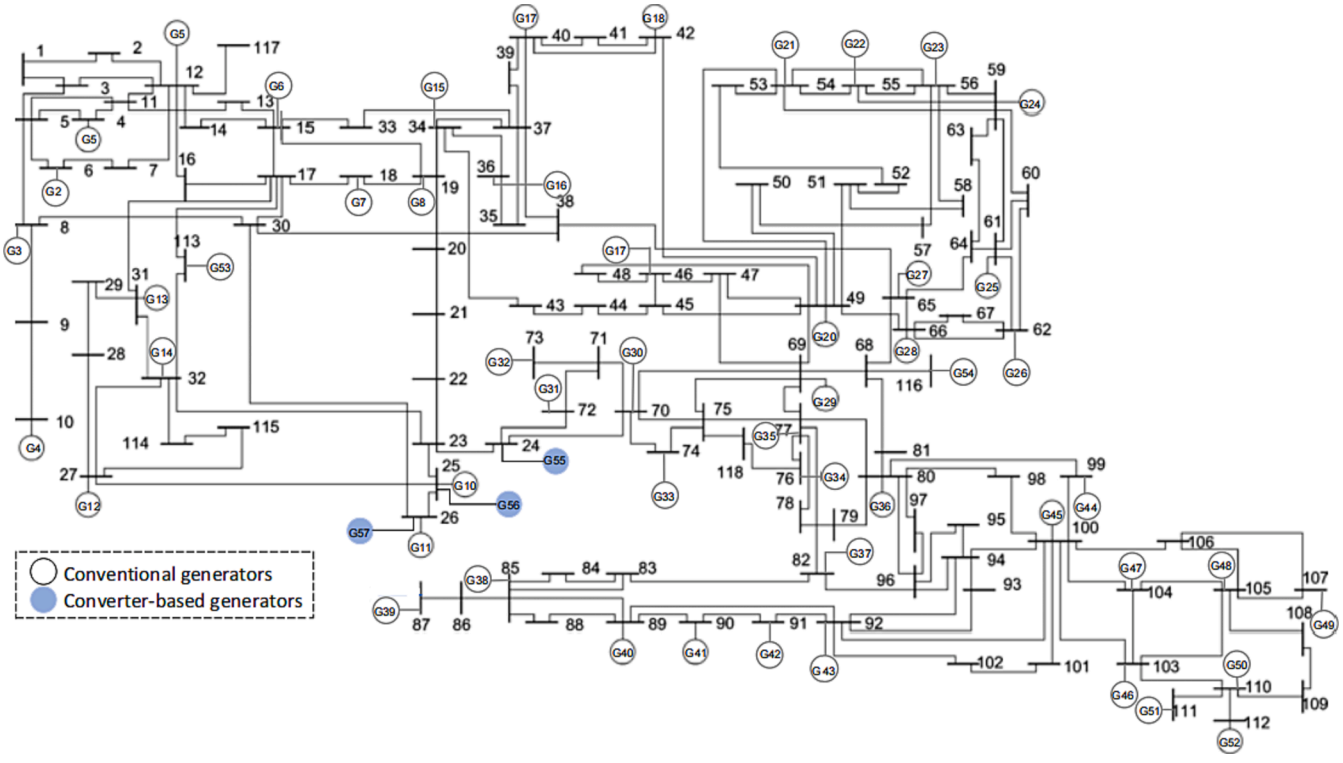

Fig. 8. The single-line diagrams of modified IEEE 118-bus test power system.

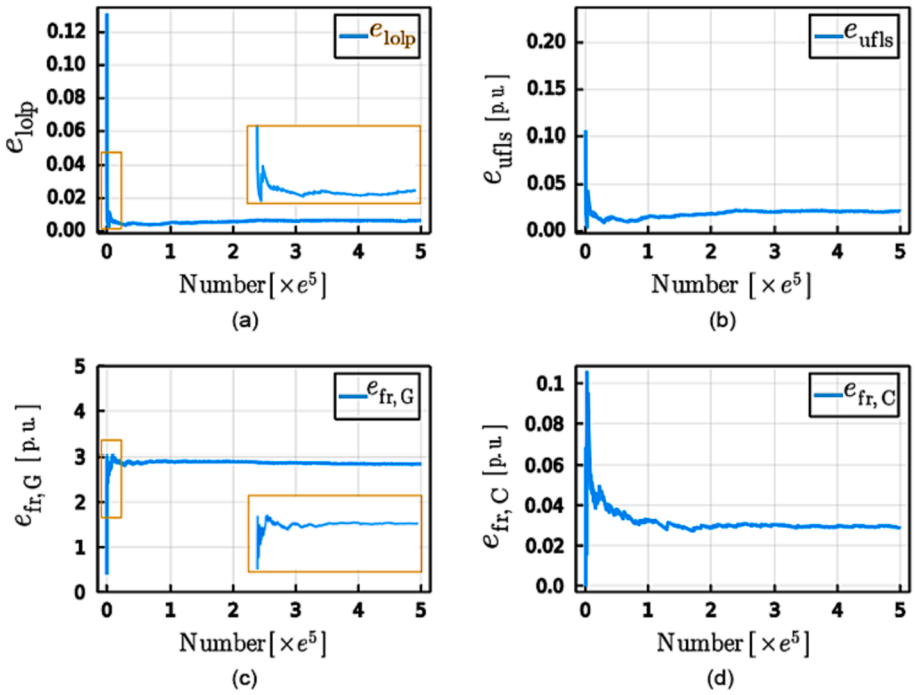

Fig. 9. The calculation process of $e_{\text{lolp}}, e_{\text{ufls}}, e_{\text{fr,G}}, e_{\text{fr,C}}$ produced by FC-CSA in the 118-bus test system.

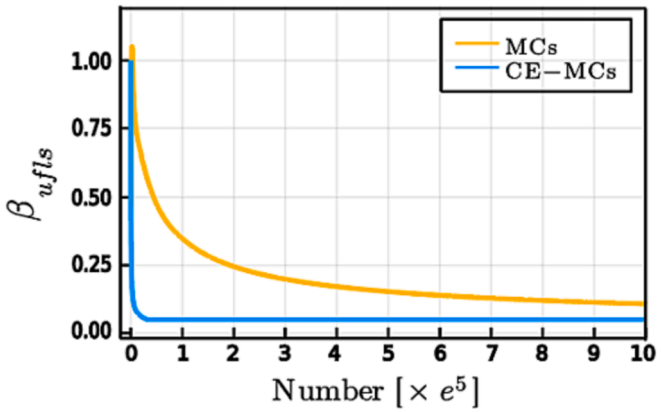

Fig. 10. The calculation process of variance coefficient by using MCs and CE-MCs concerning the proposed FC-CSA model.

utilizing T-CSA and FC-CSA are close. The difference between these models lies in the units' numbers involved in rescheduling processes (in Table 6). In the conventional model, only a part number of units is rescheduled for migrating the occurred mismatch power. In contrast, all generators through FC-CSA increase their outputs according to their FC logicisms participating in frequency regulations. It again proves the feasibility of FC-CSA considering frequency dynamics.

Also, the CE-MCs method is used to calculate the FCR allocation; their results are shown in Fig. 9. In this case, $e_{\text{lolp}} = 0.012; e_{\text{ufls}} = 0.0067$p.u.; $e_{\text{fr,G}} = 2.86$ p.u.; $e_{\text{fr,C}} = 0.308$ p.u. respectively. Furthermore, conventional MC simulation is taken as a baseline solution to test the effectiveness of CE-MCs. It can be found in Fig. 10 that CE-MC simulation has better convergence performance than MCs. Therefore, it declares the feasibility of CE-MCs for estimating the proposed FC-CSA model.

6. Conclusion

This paper presents a new FC-CSA model representing corrective rescheduling concerning contingencies, and a CE-MCs is adopted here to quantify the FCR adequacy in a wide range of stochastic contingencies. This work investigates and models the combined frequency controls from conventional synchronous generators, converter-interfaced generators, and UFLS. In this work, the jointed frequency supporting from conventional and converter-based generators and UFLS is analyzed and a refined SFR model is derived. Then, a set of mixed-integer linear constraints representing frequency dynamic requirement is constructed. To keep the rescheduling feasibility meanwhile maintain adequate FCR allocation, a new FC-CSA model is extended by integrating frequency constraints into corrective rescheduling processes under contingencies. Moreover, an accelerated CE-MCs method is used to quantify the expectation of FCR in a wide range of contingences.

Furthermore, two cases are carried out to check the effectiveness of the proposed FC-CSA model. The results suggest that:

1) The corrective result using FC-CSA is relatively conservative compared with the traditional CSA model. The reason for this difference lies in the consideration of frequency dynamic from grid-connected generators. Due to the physical restriction of frequency control and frequency regulation capacity of generators, these generators may not be able to compensate for the imbalance of power by immediately rescheduling their output. It leads to more conservation but more actual rescheduling results.
2) The corrected rescheduled result solved by FC-CSA is consistent with the change of frequency derivation. It is different from the one computed by the traditional CSA model. It is determined by the droop control strategy applied by of these generators.
3) The role of converter-interfaced generators participating in primary frequency response is analyzed. Using the proposed FC-CSA model, the FCR configuration that the power system may require under a wide range of contingencies can be estimated.
4) The efficiency of CE-MCs solution for quantifying FCR allocation under contingencies is well demonstrated.

To improve the system frequency stability under contingencies, the proposed FC-CSA model can be further strengthened to incorporate more flexible FCs of converter-interfaced generators.

Declaration of Competing Interest

The authors declare that they have no known competing financial interests or personal relationships that could have appeared to influence the work reported in this paper.

Data availability

Data will be made available on request.

References

[1] X. Zhao, H. Wei, J. Qi, P. Li, and X. Bai, "Frequency stability constrained optimal power flow incorporating differential algebraic equations of governor dynamics," IEEE Trans. Power Syst., vol. 36, no. 3, pp. 1666–1676, May. 2021.

[2] Ahmadi H, Ghasemi H. Security-constrained unit commitment with linearized system frequency limit constraints. IEEE Trans Power Syst Jul. 2014;29(4):1536–45.

[3] Shi Q, Li F, Cui H. Analytical method to aggregate multi-machine SFR model with applications in power system dynamic studies. IEEE Trans Power Syst Nov. 2018;33(6):6355–67.

[4] Tang L, McCalley JD. An efficient transient stability constrained optimal power flow using trajectory sensitivity. North American Power Symposium (NAPS) 2012;2012:1–6.

[5] Malekpour M, Zare M, Azizipanah-Abarghooee R, Terzija V. Stochastic frequency constrained unit commitment incorporating virtual inertial response from variable speed wind turbines. IET Gener Transm Distrib Aug. 2020;14(22):5193–201.

[6] Zhang Z, Du E, Teng F, Zhang N, Kang C. Modeling frequency dynamics in unit commitment with a high share of renewable energy. IEEE Trans Power Syst Nov. 2020;35(6):4383–95.

[7] Lin Y, Ding Y, Song Y, Guo C. A multi-state model for exploiting the reserve capability of wind power. IEEE Trans Power Syst May 2018;33(3):3358–72.

[8] Vrakopoulou M, Margellos K, Lygeros J, Andersson G. A probabilistic framework for reserve scheduling and N-1 security assessment of systems with high wind power penetration. IEEE Trans Power Syst Nov. 2013;28(4):3885–96.

[9] Teng F, Trovato V, Strbac G. Stochastic scheduling with inertia-dependent fast frequency response requirements. IEEE Trans Power Syst Mar. 2016;31(2):1557–66.

[10] de Magalhães Carvalho L, Leite da Silva AM, Miranda V. Security-constrained optimal power flow via cross-entropy method. IEEE Trans Power Syst, Nov 2018;33(6):6621–9.

[11] Leite da Silva M, da Costa Castro JF, Billinton R. Probabilistic assessment of spinning reserve via cross-entropy method considering renewable sources and transmission restrictions. IEEE Trans Power Syst, Jul 2018;33(4):4574–82.

[12] Leite da Silva M, Costa Castro JF, González-Fernández RA. Spinning reserve assessment under transmission constraints based on cross-entropy method. IEEE Trans Power Syst, Mar 2016;31(2):1624–32.

[13] Singhal NG, Li N, Hedman KW. A data-driven reserve response set policy for power systems with stochastic resources. IEEE Trans Power Syst Apr. 2019;10(2):693–705.

[14] Zhao Y, Tang Y, Li W, Yu J. Composite Power System Reliability Evaluation Based on Enhanced Sequential Cross-Entropy Monte Carlo Simulation. IEEE Trans Power Syst Sep. 2019;34(5):3891–901.

[15] J. F. C. Castro, P. A. C. Rosas, L. H. A. Medeiros, and A. M. Leite da Silva, "Operating Reserve Assessment in Systems with Energy Storage and Electric Vehicles," in 2020 International Conference on Probabilistic Methods Applied to Power Systems (PMAPS), Liege, Belgium, Aug. 2020, pp. 1–6. doi: 10/gmmdr3.

[16] P. Shi, Y. Li, L. Yu, X. Chen, and H. Kuang, "A Novel Spinning Reserve Partitioning Method Considering New Energy Forecasting Error," in 2020 IEEE/IAS Industrial and Commercial Power System Asia (I&CPS Asia), Weihai, China, Jul. 2020, pp. 88–92.

[17] Ye L, Jiangang Yao Xu, Ouyang XZ, Yang S. Risk Analysis and Utility Function-Based Decision-Making Model for Spinning Reserve Allocations. IEEE Access 2021;9:18752–61.

[18] Y. Cao, H. Zhang, C. Li, L. Sun, C. Li, H. Qin, Q. Guo, and Y. Zhu, "Influence Analysis of Thermal States on Dynamic Frequency Response for Power Systems with High Renewables," in 2020 IEEE Sustainable Power and Energy Conference (iSPEC), Chengdu, China, Nov. 2020, pp. 674–680.

[19] Zhao C, Wan C, Song Y. Operating Reserve Quantification Using Prediction Intervals of Wind Power: An Integrated Probabilistic Forecasting and Decision Methodology. IEEE Trans Power Syst Jul. 2021;36(4):3701–14.

[20] Paturet M, Markovic U, Delikaraoglou S, Vrettos E, Aristidou P, Hug G. Stochastic unit commitment in low-inertia grids. IEEE Trans Power Syst Sep. 2020;35(5):3448–58.

[21] Y. Zhao, S. Yang, B. Zhang, and Y. Li, "Undervoltage and underfrequency combined load shedding method," in 2019 IEEE 8th International Conference on Advanced Power System Automation and Protection (APAP), Oct. 2019, pp. 903–907.

[22] Hong Y, Chen P-H. Genetic-based underfrequency load shedding in a stand-alone power system considering fuzzy loads. IEEE Trans Power Deliv Jan. 2012;27(1):87–95.

[23] Hong Y, Hsiao C. Under-frequency load shedding in a standalone power system with wind-turbine generators using fuzzy PSO. IEEE Trans Power Deliv 2021:1.

[24] O'Malley C, Badesa L, Teng F, Strbac G. Probabilistic Scheduling of UFLS to Secure Credible Contingencies in Low Inertia Systems. IEEE Trans Power Syst Jul. 2022;37(4):2693–703.

[25] L. Ye, Z. Baohui, G. Zhe, and B. Zhiqian, "Influences of the time delay on the control effect of under-frequency load shedding in power systems," in The 27th Chinese Control and Decision Conference (2015 CCDC), May 2015, pp. 5182–5186.

[26] ISO New England Operating Procedure. Underfrequency Load Shedding Program Requirements[online]. https://www.nerc.com/pa/Stand/Reliability%20Standards/PRC-006-2.pdf.

[27] Li C, Wu Y, Sun Y, Zhang H, Liu Y, Liu Y, et al. Continuous Under-Frequency Load Shedding Scheme for Power System Adaptive Frequency Control. IEEE Trans Power Syst Mar. 2020;35(2):950–61.

[28] Wang Y. An adaptive importance sampling method for spinning reserve risk evaluation of generating systems incorporating virtual power plants. IEEE Trans Power Syst Sep. 2018;33(5):5082–91.

[29] Lubin M, Dunning I. Computing in operations research using Julia. INFORMS J Comput May 2015;27(2):238–48.

[30] Apribowo CHB, Erriyanto MF, Sutrisno S, Ramelan A. Unit commitment-security constraints using the priority list-genetic algorithm method in the IEEE 6 bus and IEEE 14 bus case studies. J Electr Eng Technol Apr. 2021;3(1):23–9.